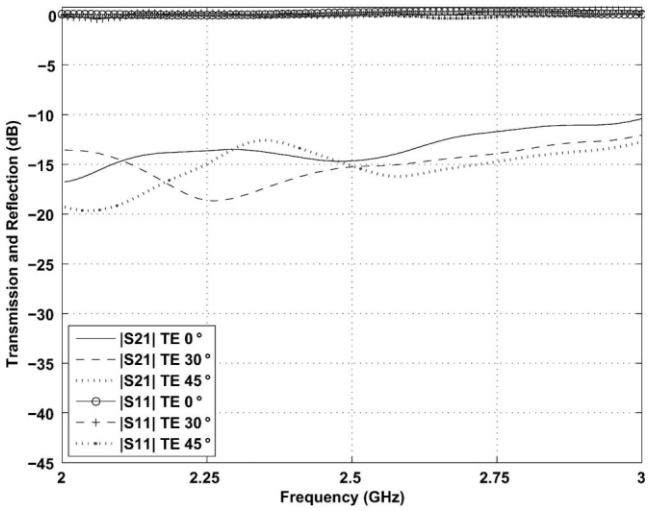

Figure 4 Measured transmission and reflection characteristics of the single-layer active FSS when the diodes are in ON state

ically, an average transmission loss of 19 dB can be achieved at the resonance frequency.

The single layer active FSS has been fabricated on a 420 × 270 mm^2 FR4 sheet (15 × 9 elements) with dielectric constant of 4.4 and 1.6 mm thickness. Figure 3 shows the measured transmission and reflection characteristics at 0°, 30°, and 45° incident angles for TE incidence when the PIN diodes are in OFF state. The resonance occurs at 2.63, 2.64, and 2.65 GHz, respectively, for 0°, 30°, and 45° incidence, while the transmission loss at these angles are 2.7, 2.8, and 3.4 dB, respectively. The reason for higher resonance is the extra inductance contributed by the connecting DC lines at the end of FSS prototype. Moreover, the main causes for transmission loss are dielectric losses, diode losses, the reflection losses due to physical presence of diodes and the soldering material on FSS surface. Figure 4 depicts the measured transmission and reflection coefficients for TE incidence when the diodes are in ON state. For 0°, 30°, and 45° incident angles, the reflection coefficient is almost 0 dB while the transmission loss is 13.1, 14.8, and 15.8 dB, respectively. Therefore, at 0°, 30°, and 45° angles of incidence, the transmission loss can be varied by 10.4, 12, and 12.4 dB, respectively, by switching the PIN diodes from OFF to ON state.

This active FSS design is not stable for parallel polarization (TM). Research is being carried out to address this issue which will be published elsewhere.

5. CONCLUSION

In this paper, a single-layer bandpass active FSS is presented. The design has shown a stable transmission response for oblique TE incidence in both ON and OFF states. An additional average transmission loss of about 12 dB has been experimentally achieved for the angles of incidence considered, by switching PIN diodes between forward and reverse bias. A further isolation can be obtained by using a dielectric with a low loss tangent and better quality PIN diodes. Besides other applications, it may find use in the intelligent Spectrum Selective Island (ISSI) applications.

ACKNOWLEDGMENT

The authors thank Professor Richard Langley, Department of Electrical and Electronics Engineering, University of Sheffield, UK, for his invitation to carry out this collaborative work on active FSS.

REFERENCES

1. B.A. Munk, Frequency selective surfaces: Theory and design, Wiley, New York, 2000.
2. T.K. Chang, R.J. Langley, and E.A. Parker, Active frequency selective surfaces, IEE Proc Part H 143 (1996), 62–66.
3. T.K. Chang, R.J. Langley, and E.A. Parker, An active square loop frequency selective surface, IEEE Microwave Guided Wave Lett 3 (1993), 387–388.
4. B.M. Cahill and E.A. Parker, Field switching in an enclosure with active FSS screen, IEE Electron Lett 37 (2001).
5. B. Philip, E.A. Parker, and R.J. Langley, Active FSS in an experimental horn antenna switchable between two beamwidths, IEE Electron Lett 31 (1995).
6. K. Mitchell, A. Keen, L. Davenport, C. Smartt, P. Leask, R. Larson, and J. Davies, Research to demonstrate the ability of close-coupled frequency selective structures to enhance the spectral efficiency of radio systems in buildings, Ofcom Project Report AY4462B, 2004. Available at: www.ofcom.org.uk/research/technology/spectrum efficiency scheme/ses2003–04/ay4462b/ay4462b1 1.pdf.

MICROWAVE VELOCITY AND IMPEDANCE TUNING OF TRAVELING-WAVE MODULATOR USING ION IMPLANTATION FOR MONOLITHIC INTEGRATED PHOTONIC SYSTEMS

Sang-Woo Seo,[1] John Yan,[2] Jong-Hwa Baek,[2] Francisco M. Soares,[2] Ronald Broeke,[2] Anh-Vu Pham,[2] and S. J. Ben. Yoo[2]

[1] Department of Electrical Engineering, City College of New York, New York, NY 10031; Corresponding author: swseo@ccny.cuny.edu

[2] Department of Electrical and Computer Engineering, University of California, Davis, CA 95616

Received 4 December 2007

ABSTRACT: *We present performance improvement in InP traveling-wave modulators (TWMs) using a periodic ion implantation on coplanar waveguide. Fabricated TWMs show the successful velocity and impedance tuning with return loss of lower than −12dB and reduced effective microwave refractive index of approximately 4 across the measured frequency range up to 50GHz.* © 2008 Wiley Periodicals, Inc. Microwave Opt Technol Lett 50: 2151–2155, 2008; Published online in Wiley InterScience (www.interscience.wiley.com). DOI 10.1002/mop.23607

Key words: *traveling-wave modulator; benzocyclobutene (BCB); coplanar waveguide (CPW); ion implantation; microwave refractive index*

1. INTRODUCTION

High-speed optical modulators are critical components in fiber-optic RF signal transmission, high-bit-rate lightwave systems, and optoelectronic signal processing. $LiNbO_3$ modulators have been widely used for these applications [1]. However, semiconductor modulators possess great potential for monolithic integration with active devices (such as lasers and optical amplifiers) [2, 3] and passive devices [4] to create compact, robust, and functional photonic micro-systems. Figure 1 shows such a monolithic integrated InP optical arbitrary waveform generation (OAWG) chip which includes 10 amplitude and phase modulators, two arrayed waveguide gratings (AWGs), and semiconductor optical amplifiers [5]. Here, a de-mux AWG splits the wavelengths of an input short pulse into 10 different waveguides, and then, each wavelength goes through an electro-absorption-based amplitude modulator and

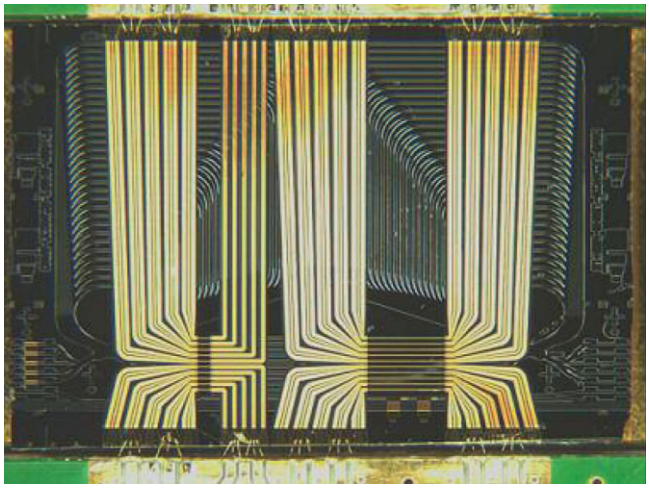

Figure 1 Monolithic integrated optical arbitrary waveform generator chip [5]. [Color figure can be viewed in the online issue, which is available at www.interscience.wiley.com]

an electro-optic-based phase modulator. Afterwards, the 10 wavelengths are multiplexed onto a single waveguide. User-specified optical waveform is generated by amplitude and phase modulation between two AWGs. In this application, high-speed amplitude and phase modulators are critical components to create truly arbitrary waveforms at an extremely broad bandwidth. Two types of modulators are commonly used on semiconductor materials: one based on a Schottky electrode configuration [6, 7] and the other based on a *p-i-n* structure. The Schottky modulator configuration shows ultra-high speed responses but is difficult to integrate with other photonic active devices on the same semiconductor substrate. Thus, the *p-i-n* modulator is the typical structure of choice for photonic microsystems [2, 3, 8, 9]. However, this structure is plagued by the thin intrinsic layer, between p-type and n-type cladding used for strong electric fields, creating a large capacitance. This large capacitance results to a low characteristic impedance (typically around 20 Ω–30 Ω) generating large signal reflections to common 50-Ω terminated microwave systems. Furthermore, the microwave velocity is typically slower than the optical velocity. For long, traveling-wave modulators, this velocity mismatch becomes the bottleneck towards higher speed modulating for low voltage operation.

In this article, we report a new approach to tune both the microwave velocity and characteristic impedance of TWMs, which is a step toward high performance monolithic photonic microsystems with RF devices. This is achieved by periodically implanting He^+ ions in p-type layer, providing the designer another option to obtain desired microwave characteristics. InP/InGaAsP traveling-wave Mach-Zehnder electrooptic modulators have been designed, fabricated and measured for this study. The design concept and simulation results of TWM using ion implantation will be first presented, and the measurement results and analysis of the fabricated devices will follow.

2. DESIGN OF TRAVELING-WAVE MODULATORS

The schematic design concept of the CPW electrodes is shown in Figure 2 where the modulator is segmented into two regions A and B; He^+ ion implantation creates vacancies in the p-InP conductive layer changing it to an insulating material. This technique results in faster microwave velocity (lower N^m_{eff}) and higher impedance are achieved in the region A. Region B is the conventional *p-i-n* structure, which typically shows low impedance. Microwave velocity in region B is much slower than optical velocity due to high capacitance formed by *p-i-n* structure.

By periodically varying the ion implantation onto the p-type layer, we have designed TWMs to increase the microwave impedance and decrease the microwave velocity. A periodic unit cell is defined and analyzed using Sonnet simulator [10]. The entire device characteristics are estimated by one unit cell and cascading its result to the fabricated device length. The material parameters for the simulation are gathered from published literatures [11-13]. Simulation results, shown in Figure 3, verify that periodic variations in regions A and B affects the Z_0, propagation loss and microwave refractive index of the *p-i-n* modulator. As more of the *p*-clad is occupied by He^+ ion implants, the microwave refractive index decreases and Z_0 increases. The drawback is a decrease in the optoelectronic modulating efficiency. However, this issue can easily be resolved by increasing the length of the modulator. Thus, the microwave propagation loss becomes the dominant affect in TWM design, and it is shown in Figure 3(b) that the total propagation loss is not significant in He^+ implantation region but in the *p-i-n* region. Thus, one can conclude that this ion implant technique can be used to adjust microwave refractive index and characteristic impedance of TWMs to improve the microwave characteristics of the *p-i-n* modulator.

3. FABRICATION OF TRAVELING-WAVE MODULATORS

The fabricated TWM is based on a Mach-Zhender interferometer (MZI) configuration using an InGaAsP/InP ridge-type waveguide with a *p-i-n* doping profile as shown in Figure 4. One arm of the optical signal transverses through the *p-i-n* structure described before. An RF signal superimposed onto the TW-CPW gold electrodes to modulate the optical carrier signal. The period of segmentation is chosen to have enough cut-off frequency to minimize the undesirable characteristics on the range of interesting frequencies due to periodic segmentation [14]. This results in periodically segmented regions of ion implanted (8 μm long) regions and with a *p-i-n* optoelectronic modulation length (24 μm long). The signal electrodes are periodically contacted on p-InGaAs layer using 3 μm wide opening of BCB layer.

The *p-i-n* InGaAsP/InP layer stacks consist of 0.1 μm p-InGaAs/1.92 μm p-InP/0.5 μm undoped InGaAsP (bandgap ~1.15 μm)/1.92 μm n-InP/0.1 μm n-InGaAs/0.6 μm n-InP/0.05 μm InGaAsP/0.1 μm undoped InP grown on semi-insulating an

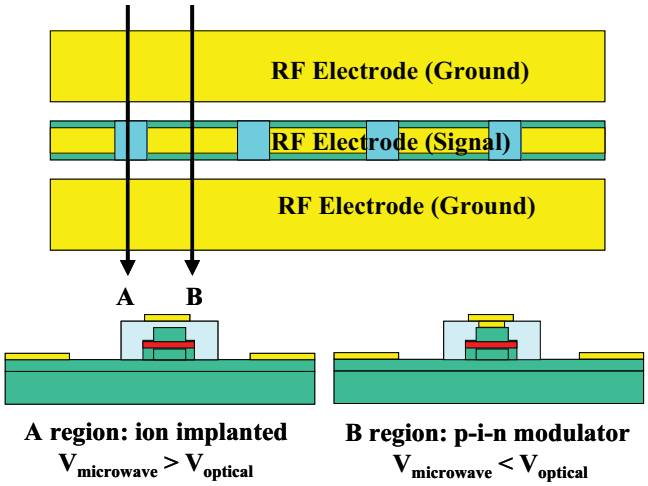

Figure 2 Design Concept of TWM CPW to optimize microwave refractive index and characteristic impedance. [Color figure can be viewed in the online issue, which is available at www.interscience.wiley.com]

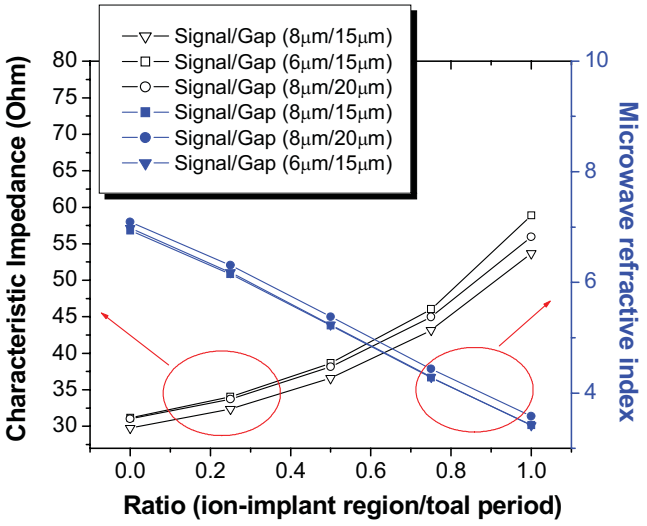

(a)

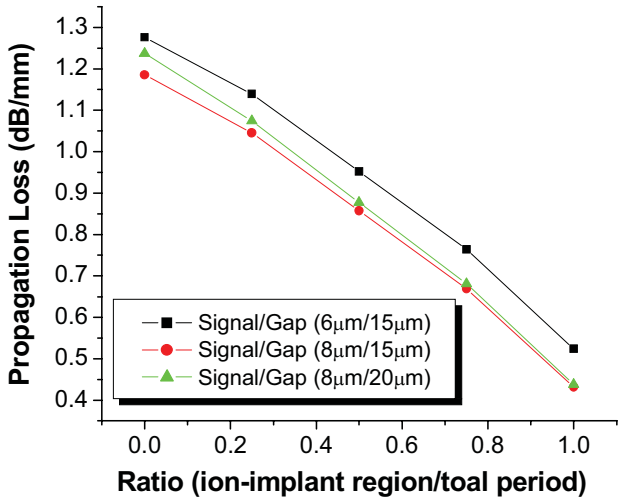

(b)

Figure 3 (a) Simulated characteristic impedance, and microwave effective index. (b) Simulated Propagation loss of TWM CPW for various signal widths and signal to ground gaps at 10 GHz. [Color figure can be viewed in the online issue, which is available at www.interscience.wiley.com]

InP substrate. Fabrication of the modulators starts with He^+ ion implantation with a photoresist mask. p-InGaAs layer of the ion-implanted region is removed before ion implantation. Doses

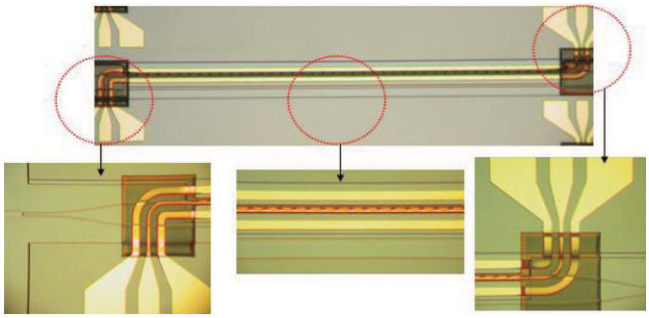

Figure 4 Top-Down photograph of the fabricated CPW on top of MZI. [Color figure can be viewed in the online issue, which is available at www.interscience.wiley.com]

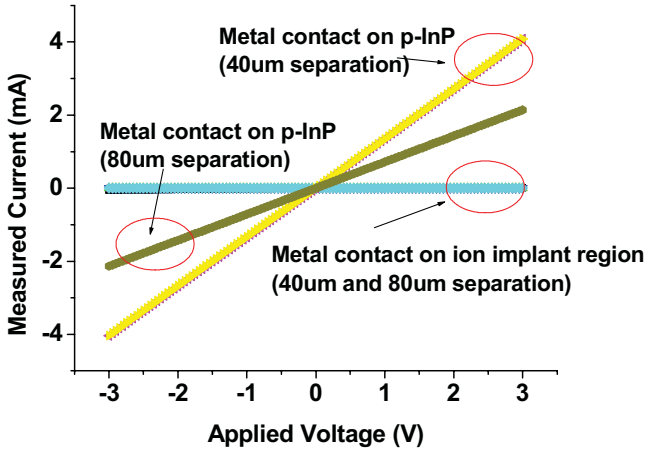

Figure 5 Measured I-V characteristics of two pads on p-InP. [Color figure can be viewed in the online issue, which is available at www.interscience.wiley.com]

of He^+ ions at different energies are carefully chosen for creating enough vacancies in *p*-InP layer using SRIM calculation [15]. After the He^+ ion implantation step, the 3 μm ridge waveguide selectively wet etched with HCl: H_3PO_4 with a SiO_2 mask. Further mesa wet etchings are used to open the *n*-contact layer and expose the semi-insulation region. Photodefinable Benzocyclobutene (BCB) is then spun, patterned, and cured at 250 C^o for 1 hour to smoothen the metal transition between the different material layers and electrical isolation. The CPW electrodes are formed by 20 nm T20 nm P μm Au e-beam evaporation and lift-off. Rapid thermal annealing is performed at 380 C^o for 45 sec to reduce the contact resistance. The signal, gap and ground width of electrodes are varied for TWM optimization. Finally, the devices are lapped and cleaved for testing. This epi-layer process is compatible other photonic devices to realize a monolithic integrated photonic system as described before.

4. MEASURED RESULTS

The conductivity of *p*-InP cladding layer, with and without He^+ ion implantation, are measured using a current-voltage measurement. *p*-InP cladding layers are mesa etched to confine the current path and He^+ implantation is performed between metal pads at different distances. Figure 5 shows the measured characteristics of two metal pads on *p*-InP with and without ion implantation. Measured resistances between two pads are around 0.73 kΩ, 1.4 kΩ, and a sub-Ohms for 40 μm, 80 μm separation and without ion implantation respectively. Measured resistances of the ion-implanted region result in a few thousands times higher than the ones of the region without ion implantation. This confirms that He^+ ion implantation was correctly performed to change *p*-InP conducting layer to an insulation material.

S-parameter measurements are performed on a Cascade probe station, using Cascade probes, and an Agilent E8364B Performance Network Analyzer (PNA). A Line-Reflect-Match (LRM) calibration establishes the reference plane up to the probe tips. N^m_{eff} has been extracted from measured S-parameters. Figure 6 shows the measured S-parameters and extracted N^m_{eff} at different biases voltages of the device: CPW parameters of the fabricated device are signal width (8 μm), separation (20 μm) between signal and ground, and ground width (20 μm). Segmented ion implantation has been performed for tuning

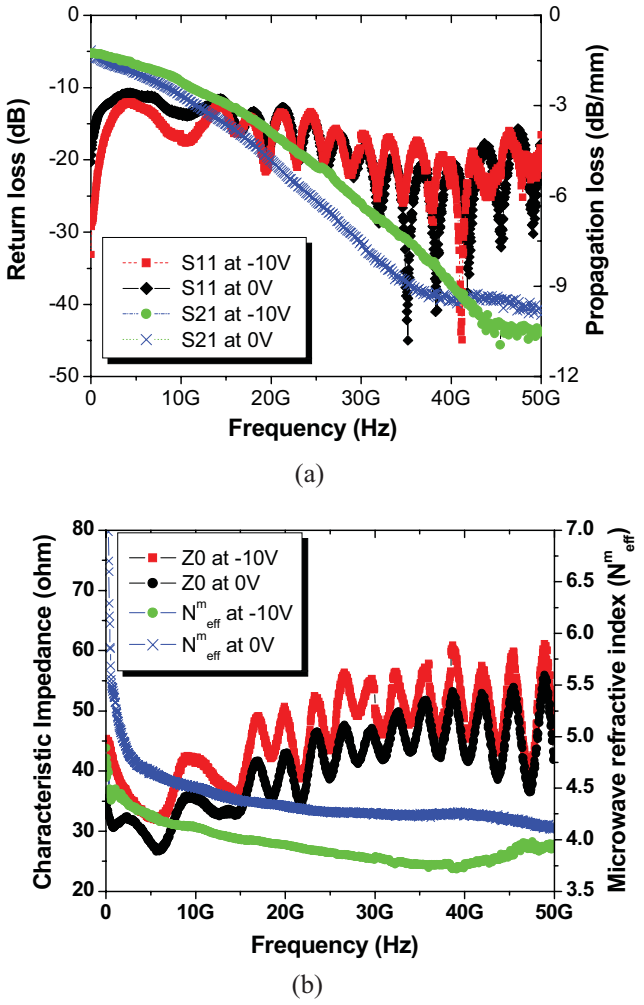

Figure 6 (a) Measured S-parameters, and (b) extracted effective microwave refractive index (N^m_{eff}) and characteristic impedance (ohm). [Color figure can be viewed in the online issue, which is available at www.interscience.wiley.com]

microwave velocity and characteristic impedance. The device has a total length of 4 mm with periodic ion-implanted regions (8 μm) and *p-i-n* regions (24 μm). Without ion implantation, N^m_{eff} was measured to be between 9 and 11 and return loss was very high (around −5dB) due to low characteristic impedance on the similar device structure. Periodic ion-implantation reduces N^m_{eff} and increases the characteristic impedance. N^m_{eff} was measured to be around 4.5 and return loss was measured to be around −11 dB at 0V bias voltage for the device with periodic ion-implanted regions (8 μm) and *p-i-n* regions (24 μm). The device performance is further improved by increasing a reverse bias. This is due to the reduced capacitance of the device when the reverse bias is increased. The measured return loss is lower than −12 dB across the entire frequency when −10 V applied to the electrodes. The extracted N^m_{eff} is also reduced when the reverse bias is increased and varies 4.1–3.7 between 10 GHz and 50 GHz at −10 V bias voltage. Theoretical optical group index for the fabricated waveguide structure is estimated to be around 3.6 at 1550 nm. N^m_{eff} can be further reduced to match an optical group index by using deep wet etching on the ridge waveguide structure or adjusting the periodicity of the ion implantation and *p-i-n* regions.

The optical propagation loss of the 3 μm width waveguide without ion implantation is measured to be about 4.1dB/cm at 1550 nm by Fabry-Perot loss measurement [16]. With periodic ion-implanted regions (8 μm) and *p-i-n* regions (24 μm), propagation optical losses were measured to be about 5.1 dB/cm at 1550 nm, slighty higher than without the ion implantation. The measured half-wave voltage (V_π) is ~7 V with a 10 dB static extinction ratio for a 4-mm device with periodic ion-implanted regions (8 μm) and *p-i-n* regions (24 μm).

5. CONCLUSION

In this article, we report techniques to increase the impedance and increase the microwave velocity of traveling-wave *p-i-n* modulators using ion implantation. We have successfully tuned the microwave refractive index and characteristic impedance to achieve the better performance of traveling-wave modulators on *p-i-n* structure. These devices are compatible with other photonic devices, such as lasers, SOAs and passive structures, to realize monolithic integrated photonic microsystems. The fabricated InGaAsP/InP TWMs with an ion implantation show improved device performance with a return loss of lower than −12 dB and reduced effective microwave refractive index to match an optical group index.

ACKNOWLEDGMENT

This work was supported in part by DARPA DSO OAWG contract HR0011-05-C-0155.

REFERENCES

1. E.L. Wooten, K.M. Kissa, A. Yi-Yan, E.J. Murphy, D.A. Lafaw, P.F. Hallemeier, D. Maack, D.V. Attanasio, D.J. Fritz, G.J. McBrien, and D.E. Bossi, A review of lithium niobate modulators for fiber-optic communications systems, IEEE J Selected Topics Quant Electron 6 (2000), 69-82.
2. S.D. McDougall, B.C. Qiu, G. Ternent, D.A. Yanson, V. Loyo-Maldonado, O.P. Kowalski, and J.H. Marsh, Monolithic integration of InGaAs/InAlGaAs-based semiconductor optical amplifiers and 10 Gb/s broadband electro-absorption modulators using quantum well intermixing technology, 16th Int Conf Indium Phosphide Relat Mater WP-25 (2004), 403-406.
3. N. Souli, A. Ramdane, F. Clevaux, A. Ougazzaden, and S. Slempkes, Tandem of electoabsorption modulators integrated with a DFB laser and an optical amplifier for short optical pulse generation and coding, IEE Proc-Optoelctron 145 (1998), 198-200.
4. S. Takeda, K. Aizawa, K. Mandai, Y. Tanaka, T. Shioda, H. Tsuda, and T. Kurokawa, 10, 20 and 30 GHz repetition rate optical pulse generation based on a AWG with integrated phase and intensity modulators, Lasers Electro-Optics, 2005. CLEO/Pacific Rim 2005. Pacific Rim Conf (2005), pp. 1200-1201.
5. S.W. Seo, F.M. Soares, J.H. Baek, W. Jiang, N.K. Fontaine, R.P. Scott, C. Yang, D.J. Geisler, J. Yan, R.G. Broeke, J. Cao, F. Olsson, S. Lourdudoss, A.H. Pham, and S.J. Ben Yoo, Monolithically integrated InP photonic micro systems on a chip for O-CDMA and OAWG applications, Photon Switching (2007), TuP6.
6. N.A.F. Jaeger, F. Rahmatian, H. Kato, R. James, E. Berolo, and Z.K.F. Lee, Velocity-matched electrodes for compound semiconductor traveling-wave electrooptic modulators: Experimental results, IEEE Microwave Guided Wave Lett 6 (1996), 82-84.
7. R. Spickermann, N. Dagli, and M.G. Peters, GaAs/AlGaAs electro-optic modulator with bandwidth >40GHz, Electron Lett 31 (1995), 915-916.
8. L. Zhang, J. Sinsky, D. Van Thourhout, N. Sauer, L. Stulz, A. Adamiecki, and S. Chandrasekhar, Low-voltage high-speed traveling wave InGaAsP-InP phase modulator, IEEE Photon Technol Lett 16 (2004), 1831-1833.
9. S. Irmscher, R. Lewen, and U. Eriksson, InP-InGaAsP high-speed

traveling wave electroabsorption modulators with integrated termination resistors, IEEE Photon Technol Lett 14 (2002), 923-925.
10. www.sonnetusa.com.
11. EMIS Datareviews Series No. 6, Properties of Indiuum Phosphide, INSPEC, London and New York, (1991) ISBN 0-85296-491-9.
12. M. Levinshtein, et al. Handbook series on semiconductor parameters, world scientific, (1996) ISBN 981-02-1420-0.
13. www.cyclotene.com.
14. R. Spickermann and N. Dagli, Experimental analysis of millimeter wave coplanar waveguide slow wave structures on GaAs, IEEE Trans Microwave Theory Tech 42 (1994), 1918-1924.
15. www.srim.org.
16. R.G. Walker, Simple and accurate loss measurement technique for semiconductor optical waveguide, Electrons Lett 21 (1985), 581-583.

A 24-GHZ ACTIVE SPST MMIC SWITCH WITH INGAP/GAAS HBTS

Jong-Ryul Yang,[1] Dong-Wook Kim,[2] and Songcheol Hong[1]
[1] School of Electrical Engineering and Computer Science, Division of Electrical Engineering, Korea Advanced Institute of Science and Technology, 373–1 Guseong-Dong, Yuseong-Gu, Daejeon, Republic of Korea 305–701
[2] Department of Radio Science and Engineering, Chungnam National University, 220 Gung-dong, Yuseong-Gu, Daejeon, Republic of Korea 305–764; Corresponding author: yuri102@ kaist.ac.kr

Received 4 December 2007

ABSTRACT: *A 24-GHz single-pole, single-throw (SPST) switch with high isolation is designed using InGaP/GaAs HBT process. To obtain high isolation in an off state, cascode structures are utilized and an additional shunt transistor is introduced in an output, which helps to reject a leakage signal. Dummy cascode structure is used as a current steering circuit for input matching and short rise/fall time. The fabricated SPST switch shows an effective isolation of ~52 dB at 22.8 GHz and 41 dB at 24 GHz.* © 2008 Wiley Periodicals, Inc. Microwave Opt Technol Lett 50: 2155–2158, 2008; Published online in Wiley InterScience (www.interscience.wiley.com). DOI 10.1002/mop.23606

Key words: *SPST switch; active switch configuration; high effective isolation; UWB signal generation*

1. INTRODUCTION

Recently, a signal generation block for keeping a wideband characteristic and generating pulse signals efficiently is one of the most important research topics in UWB radar sensor [1]. There are two general methods for the signal generation; one is to generate pulse signals directly using pulse generator or impulse generator, and the other is to use a high speed switch together with a conventional CW signal generator to shape the pulse signal [2]. The latter makes it possible for the radar sensor to operate in FMCW and pulse modes [3]. The important characteristic of the switch required in the signal generation block is isolation because isolation between input and output ports decides the power of a leakage signal when the switch state is off. Because of the limited isolation level, high frequency signals can be transmitted in the unwanted time and the pulse shaping is not properly performed for the radar sensor [4]. In addition, Tx output spectrum violates the Federal Communications Commission (FCC) spectrum mask regulation when Tx leakage signal is over −40-dBm signal power.

In this work, a scheme to place an additional shunt switch at the output load path of cascode type active SPST switch is proposed to improve the isolation characteristic at 24 GHz. The measured results of the proposed switch show the best isolation performance among the active-type SPST switches.

2. SPST SWITCH FOR HIGH ISOLATION

While conventional passive-type switch has high isolation between input and output ports in an off-state and high power capability, it also includes an insertion loss. Moreover, it cannot be applied for the UWB pulse generation using CW signals due to the limit of operating speed. Compared with the passive-type switch, the active-type switch can operate with faster operating speed [5].

Figure 1 shows a schematic of the proposed SPST switch. The switch consists of seven transistors. A turn-on voltage of InGaP/GaAs HBT in the designed circuit is 1.24 V. In the on-state of the switch, control voltage "+Vcont" in Figure 1 is set up to be 1.5 V, and "−Vcont " in Figure 1 is set up to be 1 V. Then Q_1, Q_3, and Q_5 are operating in an on-state and Q_2, Q_4, Q_6, and Q_7 are operating in an off-state as shown in Figure 2(a) because the bias control voltage of Q_2 is lower than the turn-on voltage of a transistor. Q_2, Q_4, and Q_6 as dummy transistors do not have an effect on the switching operation. Input impedance is determined by a parallel circuit consisting of turned-on Q_1 and turned-off Q_2. In the on-state, the SPST switch is operating as a cascode amplifier, so the switch has a voltage gain while a conventional passive-type switch has an insertion loss. In the off-state, Q_4 turns on and Q_3 turns off due to the applied control voltages. So Q_1 and Q_5 are off, Q_2 and Q_6 are on as shown in Figure 2(b). RF input signal is ideally bypassed to the ground and it's not transmitted to output port. But in a real world, the RF signal is transmitted to output port through transistor parasitic. Because the cascode transistor makes high isolation between input and output ports in the off-state, a leakage signal can be decreased greatly [6]. Additional transistor Q_7 in output load is controlled by "−Vcont" and it provides a leakage signal path, which results in the isolation improvement of the switch. Because the input impedance is almost same, regardless of the switch states, the reflected signal power is almost constant in any state of the switch. When the reflected signal power varies with input impedance unsettled by the switch operation, the power spiking can be generated and can damage the signal source. To minimize the switching time, the current steering technique is used for the switch design [7]. Q_2, Q_4, and Q_6 are dummy transistors for the current steering technique of high-speed operation.

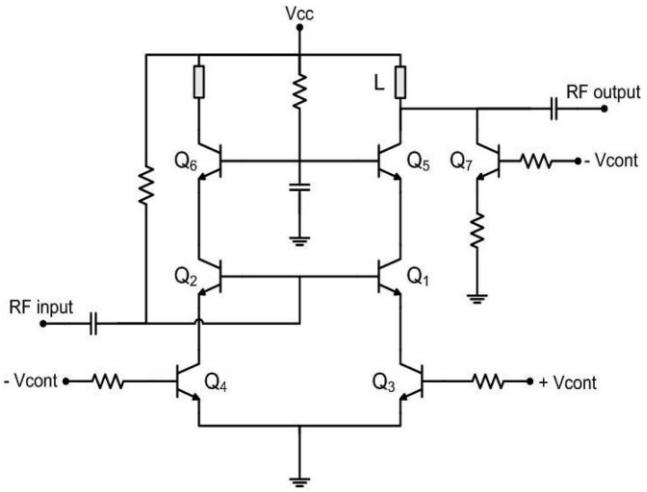

Figure 1 A schematic of the SPST switch with high isolation using HBT process